Ilkogretim Online - Elementary Education Online, 2021; Vol 20 (Issue 5): pp. 9111-9135
http://ilkogretim-online.org
doi: 10.17051/ilkonline.2021.05.1001

Analytical Investigation of Ribbed Channels for Gas Turbine

Seemant Girdhar, Department of Mechanical Engineering, R D Engg. College, Ghaziabad, U. P., India, 201206, Email: seemant.girdhar@gmail.com

Abstract
In this study, a ribbed surface in an interior channel of a stationary turbine blade is benchmarked computationally and validated using experimental data. In order to investigate the CFD conjugate heat transfer and duplicate a model from a published article, STAR-CCM+ was used to find the turbulence model that best matched the published experimental values. An internal experimental rig was confirmed by comparing convective heat transfer coefficients and pressure profiles using those computational parameters and the CFD results. When compared to a smooth channel, this cooling technique improves turbulent mixing by detaching and reattaching the boundary layer, increasing heat transfer. The general objective is to assess a practical cooling technique while taking into account the flow physics, efficient heat transfer rates, and channel pressure drop reduction. The V_2f turbulence model produced the closest matches to the experimental results, however EBk- turbulence model was employed for initial testing because to its instability at high Reynolds number. Shorter reattachment lengths and higher Nusselt number values between the ribs were the results for EBk-turbulence. The reported results' 6.8% and 6.66% respective levels of uncertainty are met by both the heat transport and friction components. Benchmark computational results will support the experimental setup's validity for further optimization and testing of various rib arrangement configurations.

Keywords : CFD, STAR-CCM+, Nusselt number, EBk-Turbulence

1. INTRODUCTION

There is more room for its manufacturing because to the ongoing need for energy and power. Today, a variety of power generation methods, such as land-based, water-based, and air-based methods, are widely used. The gas turbine engine, which is used to power practically all modern aircraft as well as land-based power plants, is one of the most widely utilised devices to create huge amounts of power. Such enormous masses are propelled into the air with the aid of the conversion of thermal energy into work (thrust). The Brayton cycle, which includes compressing air, creating heat, and turning that heat into work to propel the aircraft, forms the basis for gas turbine engine operation.

Continuous improvements in aviation engines have only served to boost their efficacy, create better, more aerodynamically sophisticated parts, reduce total weight, enable long-distance flight, etc. The temperatures of these adiabatic flames, which range from 1500 to 2000 °C, are higher than the melting points of the majority of the materials used to cast engine blades and other components. Therefore, internal cooling is crucial to ensure that turbine blades are used to their full potential without having to be replaced frequently because raising the turbine inlet temperature improves the gas turbine's efficiency. Due to the complexity of various cooling systems and the rate at

which it needs to be cooled, internal cooling has limitations.

Thermodynamics

An isentropic Brayton Cycle process, which comes after an open cycle phase, controls how well a gas turbine performance Fig. 1.1 presents a fundamental of Brayton cycle.

As seen in the Brayton cycle, the ambient air enters the compressor where the air is compressed and the air pressure is raised considerably. In the combustion chamber, this compressed air is then combined with fuel and fired, adding heat.

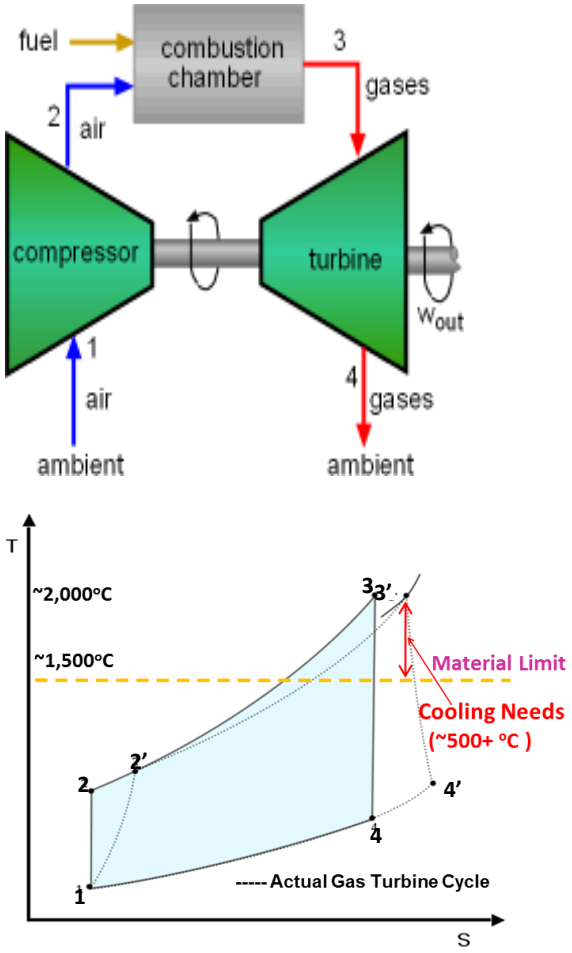

Fig.1.1 IdealBraytonCycle

This air then turns the compressor's associated turbine, which in turn turns the compressor. When using the current standard fuels, the adiabatic flame temperatures that leave the combustion chamber range between 1500 and 2000 °C. The majority of materials used to construct the turbine blades and the surrounding casing are unable to endure such high temperatures. At temperatures of 1100 °C or less, the employed super alloys fail. The T3, or turbine inlet temperature, is significantly dropped due to material restrictions, which lowers total efficiency.

The Braytoncycle efficiency is given by:

$$\eta = 1 - \frac{T_4 - T_1}{T_3 - T_2} \qquad (1)$$

Although the regulating Brayton cycle has many performance advantages, it has also experienced numerous inefficiencies over time. Mechanical losses, compressor losses, and expander losses are a few of the few factors that have an immediate effect on the

system's overall work output.

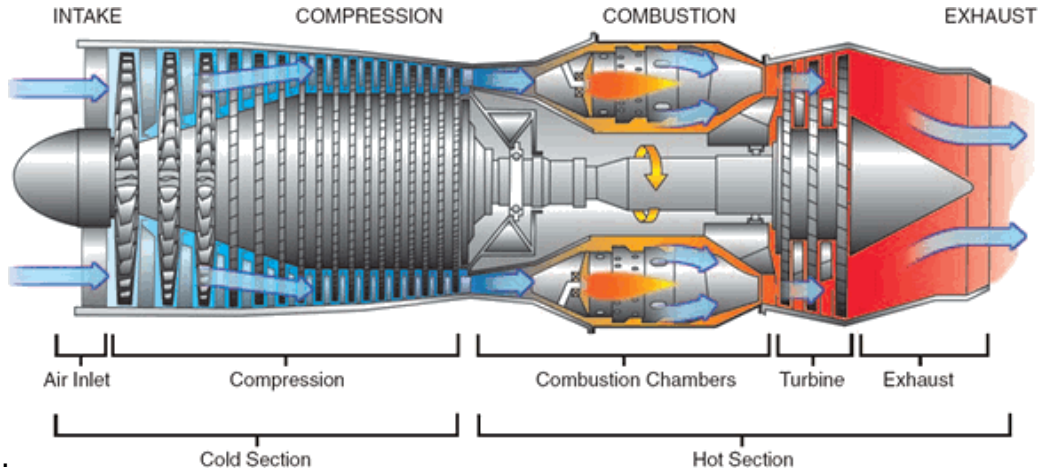

Fig. 1.2 Stagesof a Gasturbineengine(Wikipedia)

As seen in Fig. 1.2, mainly the first stage of the turbine experiences very high heat loading as it is directly situated after the combustion chamber, thus having high internal heat transferrates isamust.The air that is removed from the compressor is about 650°C, and when it comes into contact with the hot gases, it reduces the temperature of the blades to around 1000°C, which is acceptable for the engine to run reliably. It is obvious that excessive air bleeding reduces the system's effectiveness. Therefore, the correct amount of bleed air is needed to maximise the cooling effect while minimising metal failure. This is very wellhighlighted by the fact that a 56 Kelvin increase in hot gas temperature potentially yieldsan increase of up to 13% in power output or 4% in simple cycle efficiency (HyungHee,2011). The turbine blades experience significant thermal strains and thermal loads as a result of these high temperatures. So, one of the key elements in extending the overall life of the aeroplane engine is turbine cooling.

Turbine Blade Cooling

One of the simplest solutions to meet the always increasing need for smaller, lighter, and more efficient gas turbine engines is to raise the temperatures at the inlet of the turbine. Therefore, meeting those objectives leads to advancements in the turbine cooling industry. Thus, efficient and precise cooling systems are required. If the metal blade's temperature forecasts are off by merely 30oC, the life of a turbine blade can be cut in half. The designers must correctly forecast the regional airfoil metal temperatures and local heat transfer coefficients in order to prevent premature failures or catastrophes.Mitigate local hot spots, which are a significant contributor to material failures, as this is another technique to lengthen the life of the blades. The ability of turbine blades to withstand high temperatures, severe stress loads, and significantly shifting climatic conditions has improved over the past few decades, extending the life of the entire machine.

Rib-Turbulated Channel Cooling

Ribs are regulated protrusions that are positioned along particular target walls of the internal duct. To improve heat transfer, rib turbulence promoters are repeatedly cast on the interior duct's opposing pressure and suction walls. Ribs on the opposing walls maximise the interaction between the coolant and wall and aid in efficiently cooling the turbine blade. Because they must match the external thermal loads, which differ for the

pressure and suction sides, in some circumstances the duct only has ribs on one side.Its disadvantage is pressure drop, which will be higher than in a typical smooth channel, even though it generates friction for the flow in the channel, which is associated to increased heat transfer. Therefore, it's crucial to have the proper rib height, rib pitch, and angle at which the ribs contact the flow to minimise pressure loss and maximise benefits.

LITERATU REREVIEW

The intake temperatures of gas turbines have risen over time thanks to continuous cooling techniques. The metallurgical limits to withstand the hot gases have not yet reached the highest feasible temperatures, despite advances in super alloys. Therefore, component cooling is necessary to maintain a balance between rising turbine input temperatures and improving system efficiency. Boyce (2006) noted that the annual rise in turbine firing temperatures due to material advancements has only been 4^{o}C. While improved cooling methods were responsible for the 11°C annual increase in turbine inlet temperature.

To improve heat transfer, turbulence promoters are added to the internal cooling route. The so-called rib-turbulators, which are normally oriented at an angle transverse to the flow direction and created as an integral structural part of the airfoil inner wall, are the most frequent turbulence promoters. Over the years, several investigations have been carried out utilising a variety of experimental approaches on a wide range of rib topologies in various sized cooling channels.The mid-chord region of an airfoil is often cooled by rib-turbulators, which are typically cast on both walls of internal cooling passageways with two-dimensional structures. The literature on rib-turbulated cooling in non-rotating channels is extensive and covers a wide range of combinations of rib height, rib angle, rib spacing, rib form, and inline or staggered rib configurations.

Typically, the rib height to hydraulic diameter (e/D) ranges by about 5-10% of theentire cooling passage, the rib spacing-to-height ratio also known as the Pitch-to-heightratio (P/e) varying from 5 to 20, and a rib flow attack angle around 30˚-60˚ in addition tothe 90^{o} flow which is perpendicular to the mainstream flow (Han, 2006). It is claimed that smaller ribs are more effective for flows with higher Reynolds numbers, however because of the high speeds, the improvements in heat transmission decline. Additionally, for flows with higher Reynolds numbers, the friction factors rise, increasing the penalty for pressure decrease.

J.C. Han (1988) looked at orthogonal and angled ribs and found that positioning ribs at an angle to the channel's main flow would result in a higher rate of heat transfer than placing them at a 90o angle. This is also backed by various other studies byHanandPark(1988)andParketal.(1992)wheretheyinvestigatedthethermalperformanceof angled ribs compared to orthogonalribs.

In a rectangular rib-roughed passage, the effects of rib configurations on heat transmission and flow behaviour were examined by Kiml, Mochizuki, and Murata in 2001. In the study theymodeled a 2:1 aspect ratio rectangular channel with four configurations of angled ribs(90^{o}, 75^{o}, 60^{o} and 45^{o}). the oblique ribs should be positioned that is why along the ribs second flow strikes on the top wall and carry to bottom wall the cold air from passage. They came to the conclusion that the secondary flow's great rotational momentum was the reason why the 60-degree rib design managed to transfer the most heat.

Han etal.(2000) mentioned that insome highly demanding cooling designs,larger rib height-to-channel hydraulic diameter ratio can be used to generate higher heattransfer

enhancement provided pressurepenaltyis not amain concern.
Rauetal.(1998)measuredthelocalheattransferperformanceinaribbedroughened square channel with blockage ratio (rib height-to-hydraulic diameter of thechannel – e/D) of 10 to 20%. The local heat transfer distributions on the smooth side walls exhibit substantial gradients in the three-dimensional flow field created by the strong secondary flows, the researchers discovered. They came to the conclusion that the correlation which utilized heat transfer in ribbed channel to smaller e/D ratio to apply the greater e/D ratio.
EkkadandHan(1997)studied heat transfer distributions in two passsquarechannelswithribturbulatorsusingatransientliquidcrystaltechnique.We discussed four angles 60º parallel, 90º parallel, 60º V- shaped, 60º - Inverted.Theynotedthattheperiodicribsbreakthelaminarsublayerandcreatelocal wall turbulence due to flow separation and reattachment between the ribs, greatlyenhancingtheheattransfer(Ekkad,1997). They discovered all ribbed channels, and highest Nusselt number ratio above the ribs, and lowest before and after both.
Han, et al. (1991) studied the effect of the rib angle orientation on local heattransfer distributions and pressure drop in a non-rotating square channel with opposite,in-line ribbed walls. The shape discovered 60º and 45º V-shaped and 90º transverse in terms of performance.“TheV-shapedribproducesthehighest heat transfer augmentation while the inverted V-shaped rib generates the greatestpressuredrop”(Han et al., 1991).
Rib turbulators started concentrating on researching "high performance" ribs. Han and colleagues (1991) investigated a square channel with parallel (angled), crossing, and V-shaped ribs. They demonstrated that the parallel ribs 45º, 60º inferiority to V-shaped.
Wang et al. (2001) performed experiments to study the local heat transfer andpressure drop characteristics of developing turbulent flows of air in three different typesofribbedducts.These include the square ducts with constant cross sections, diverging square ducts, and convergent square ducts. The diverging duct displayed the highest heat transfer characteristics when the three ducts were analyzed, it proves that duct cross-section performs better to convergent duct.
Another study for heat transfer and friction losses in a square channelwith 90ºribs on one, two, three and four walls was conducted by Chandra et al. (2003). The Reynolds values used in the trials ranged from 10,000 to 80,000. It was discovered that the thermal performance declines with an increase in ribbed walls due to an increase in pressure drop.
Turbulence is greatly influenced by the Pitch, which is the distance between the trailing edges of the two ribs that follow one another. It has an impact on the flow's dissociation and reattachment, which has an impact on the channel's improved ability to transport heat. Han et al. (1978), has experimentally showed that the maximum heat transferis obtained for Pitch-to-rib height ratio (P/e) of 10. The reattachment between the ribs was not noticeable below this value. Figure 2.3 illustrates the flow phenomenon of detachment and reattachment for various P/e ratios. The boundary layer and separating bubble each rib for P/e values lower 7 separate zone and ribs not equal to. The re-attachment occurs between the ribs when P/e is equal to 10, which is thought to be the ideal number since heat transfer is maximum to accomplished and separate bubble on top of ribs which extend the back with separation after rib. This is P/e at near wall flow 10,the near wall flow breaks up to its maximum extent, increasing turbulence and improving the exchange of fluid between the near wall region and the core flow.
Buchlin, (2002) studied the convective heat transfer in a channel with perforatedribs. In order to forecast the highest heat transfer, he modelled several perforation kinds in a

single rib turbulator. The mapping of heat transfer coefficients was done using infrared thermography and a thin foil that was steadily heated. In-depth research was done on the Chevron type of perforation. Reynold's number above 20,000 and the open-area ratio of the perforated rib up to 36 percent were shown to greatly improve heat transfer.

Kim, Rhee et al. (2004) investigated the duct aspect ratio effects on the masstransfer in a rotating duct with 90^{o} ribs where they show that the Sherwood number ratioare 2.5 times higher than the fully developed values in a stationary smooth pipe due to theflow reattachment near the ribbed surfaces. They continue by demonstrating how the increased rib height-to-duct height ratio results in improved mass/heat transfer in a duct with a greater aspect ratio. However, when the duct aspect ratio increases, that becomes significant in turning region and rotational on mass/ heat transfer.

This study is in ribbed cooling, duct aspect ratio and rough cooling have been conducted. According to a survey of the literature, little work has been done to develop ideal turbulence models for interior channels with rib roughness that is accurately reflect experimental conditions. This is as a result of complex fluxes and geometrical restrictions within these cooling channels.

The primary goal of this research is to boost gas turbine efficiency while improving power output. Therefore, it's crucial to improve the rate of heat transmission within the channels in order to increase efficiency. Therefore, it is crucial to compare experimental results with CFD in order to create precise computer models that accurately reflect the flow conditions in a real gas turbine. By lowering the cost of experiments and producing more reliable results, this aids in further research. Therefore, one of the objectives of this study is to investigate several industrial turbulence models. In the following chapter, certain goals and objectives will be covered in more detail.

METHODOLOGY

The goal of study expressed many computational turbulence models which employed in comparing the existing experimental correlations. The geometrical duplicate facility in gas turbine is to be created in gas turbine. CFD data based in house experimental rig is validated. A schematic of the objectives of this project is shown in Fig. 3-1 below.

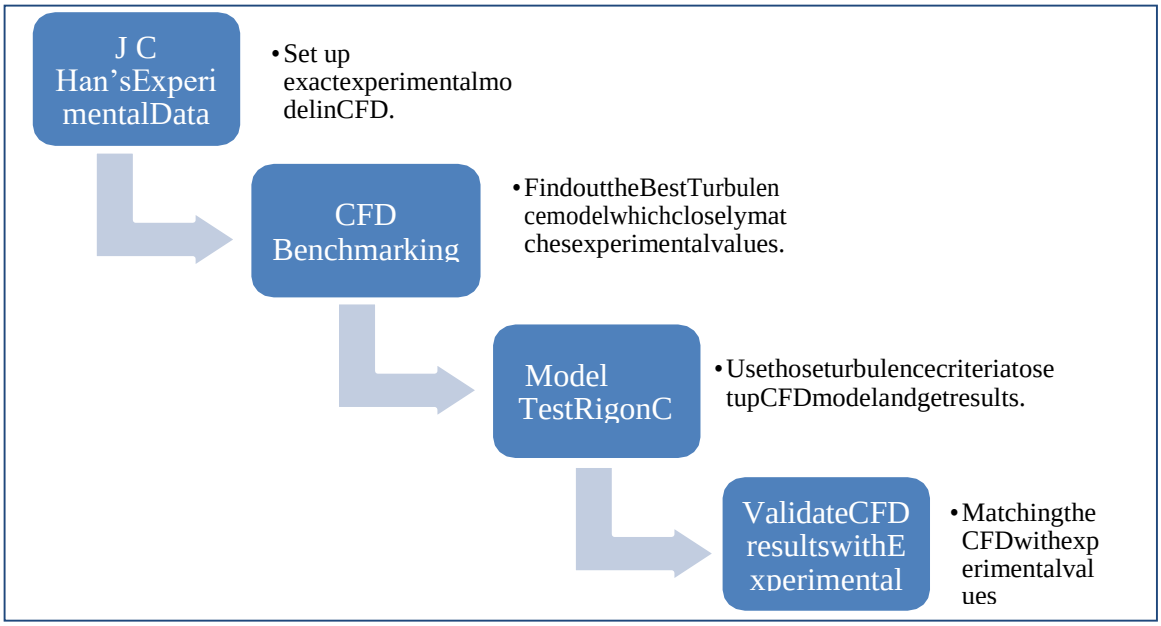

Fig. 3.1 Flowchart of the goals of this project

A experimental and analytical study of smooth channel was conducted in order to assess heat transfer in inserted ribs. For the single periodic ribs channel the CFD and experimental study was done additionally.

Computational Setup

The majority of the research was done using numerical analysis, but computational fluid dynamics was a crucial tool in designing the intricate the gas turbine for the cooling configurations to forecast physics and heat rate. When building effective enhanced heat transfer channels, it is more preferable to use 3D flow findings from CFD than single measured sites from experiments. This work was utilized Star-CCM+ to all CFD mesh generation, post processing data, and construction geometry.

Model Set-UP and computational region

To duplicate the experimental work done by J.C. Han, J.S. Park, and C.C.Lei, a computational model is being set up (1985). In this paper, experimental comparisons of distinct rib shapes observed at a range of different Reynolds numbers are validated computationally.

The model setup for this case in particular is a rib roughed surface with periodicribs on both sides. The entire system is 3.048 m long and is made up of two main sections: a 1.524 m long unheated inlet duct and a second channel of the same length with heaters installed in them to provide a steady heat flux on the bottom walls with ribs. The duct had a 0.076 m-side square shape. The rib pitch-to-height ratio was 10 and the height-to-hydraulic diameter ratio was e/D = 0.063, indicating that the rib size and spacing were non-dimensional. This ended up giving a square rib of side 0.00476 m. Fig. 3.2 below gives the channelsetupwhich was replicatedfromHan's(1985)work.

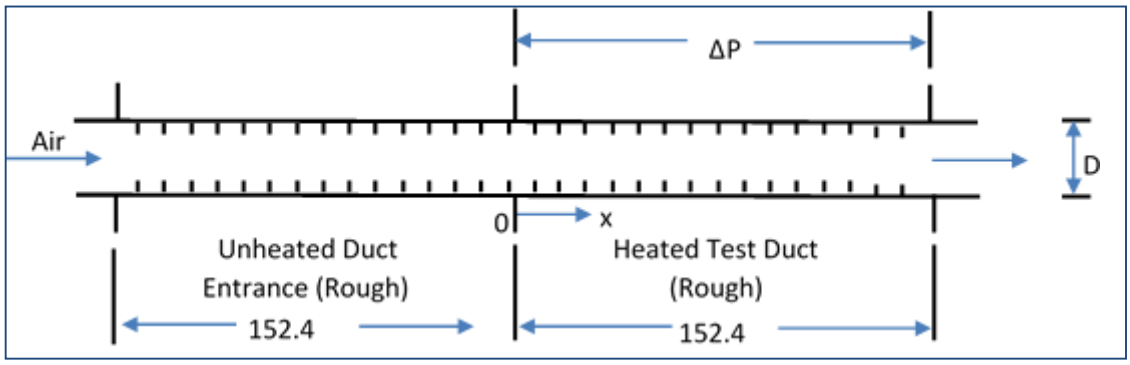

Fig.3.2 Representation of the channel setup

As bottom and top are in touch with primary heat and fluid flow outside, adding ribs to both sides of the wall will boost heat transmission between them. In order to extract additional heat, ribs on the opposing walls of the channel promote heat transfer. The local mean bulk temperature (Tref), which was determined using the energy balance, was used to calculate the heat transfer coefficients. Based on the inflow velocity, regional fluid characteristics, and hydraulic diameter, the Reynolds number was estimated.

The geometry was produced in full scale to eliminate any errors in the computational model's setup. On top wall a symmetry surface was made on top of rib and another on side wall to duplicate another portion of the ribs, simplifying the computation and modelling only one-fourth of the actual rig. Fig. 3-4 below illustrates this.

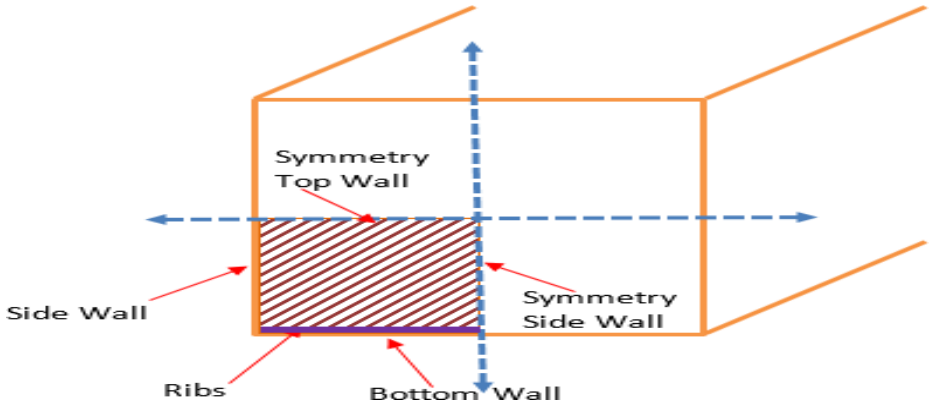

Fig.3.3 CFD sectioned model

There were two sections in the domain, each with 33 ribs on the bottom wall. Outlet from unheated area of duct to inlet was used to determine flow rates followed by outlet pressure. At the inlet, a field function was developed to produce 4.452 m/s velocity and 21500 reynolds number. Temperature change within the rig is made possible by the heated portion of the rig's continual heat flux. 1650 W/m2 was chosen as the heat flux. The study's analysis involves a 90o instance in which the ribs are perpendicular to the direction of the primary fluid flow. The domain that is configured in STAR-CCM+ Ver. 9.02.007 is shown in Fig. 3-5 below. To display the internal section of the ribs, the top and side symmetry walls have been obscured in the image.

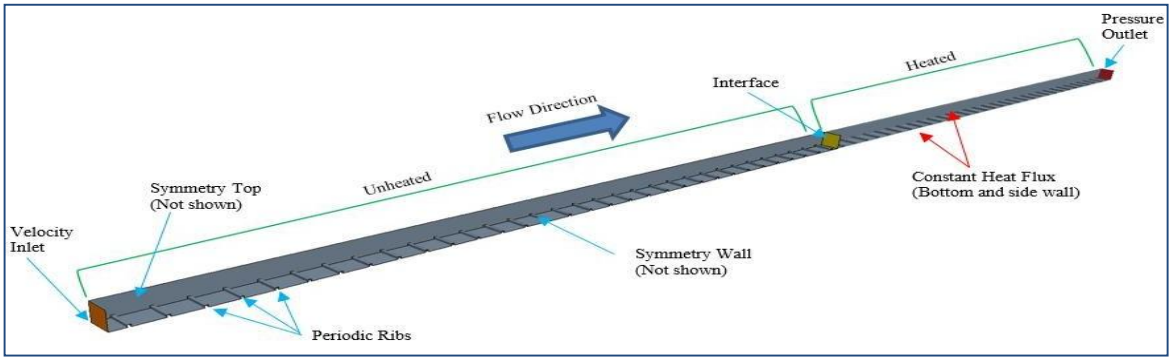

Fig. 3.4 DomainSet-up

Turbulence meshing

The sides were coarser while ribs and bottom wall were highly meshed, due to the relevance of the portion and its function in heat transfer. This was done with the understanding that the cell sizes in the two sections do not differ much. The effects of the normal temperature gradient and the boundary layer were captured using polyhedral elements with prism layers and surface wrapper mesh types. The finer region's mesh size was adjusted at 0.6 mm polyhedral elements with 20 layers of prisms close to the margins (2mm thick). The total number of cells in the entire mesh came to around 29 million cells. The mesh transition between the two sections as well as the mesh on and around the rib are depicted in Fig. 3.5 below.

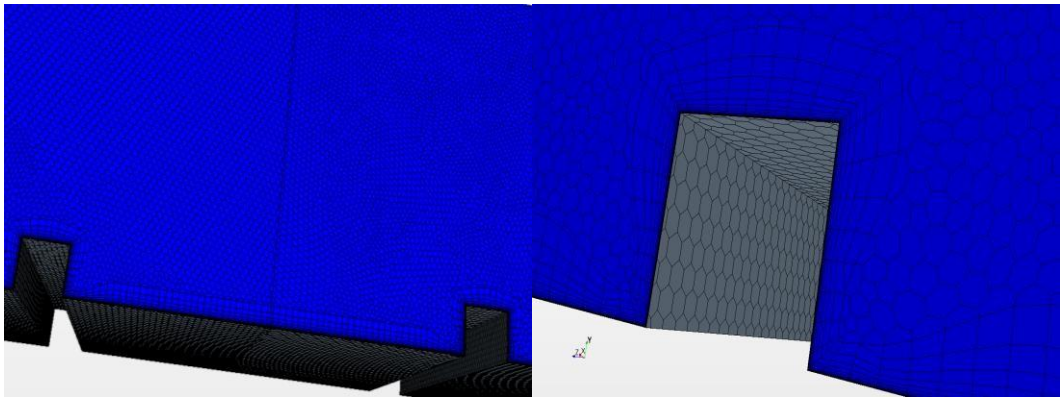

Fig.3.5 Mesh sizes and cell quality around the rib

Through the use of STAR- CCM+, a mesh independence investigation was conducted. In STAR-CCM+, a base size is described as setting several parameters, such as target area/size, thickness of boundary layer etc. Therefore, just the base size must be modified to refine or coarsen the mesh, which will automatically modify the desired values. Running multiple examples at various base sizes enabled mesh independence to be attained. The three instances in Fig. 3.7 below have bases that are 0.9 mm, 0.6 mm, and 0.45 mm, respectively, for a about 7.9 million, 28.9 million and 56.4 million of total cell. The computational rig's heated and cooled surfaces are both counted in this total cell count. In these three situations, the average surface temperature and the average Nusselt number on the bottom wall were compared to determine which had the smallest difference. The temperature change between the 0.9mm and 0.6mm cases is 3.6 percent, but only 0.14 percent between the 0.6mm and 0.45mm cases, as seen in the figure. The Nusselt statistics also show a similar pattern, with 6.2 percent between the first two cases and 0.12 percent between the second two cases. Since similar results were observed without the requirement for a finer mesh, using the second case with a 0.6mm base size is therefore more effective. A mesh independent case is crucial since it aids in choosing the appropriate mesh size, which in turn speeds up computation. The Rk-turbulence model underwent a mesh independent analysis.

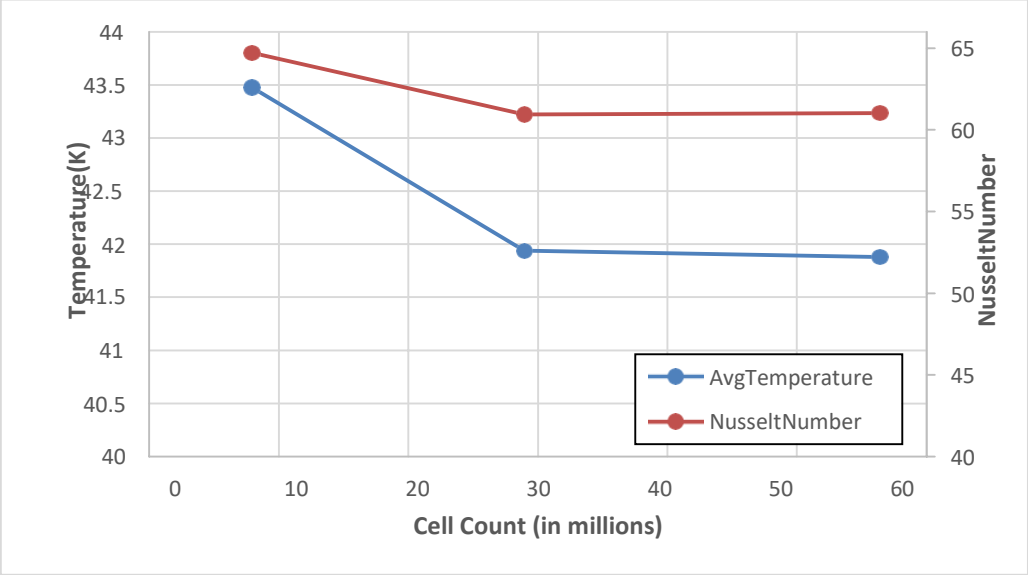

Fig. 3.6 mean surface temperature vsNusselt number

A flow that is wall-bounded has a non-dimensional wall distance of Y+. Within the boundary sub-layer, it is utilised to record wall effects. The following equation yields Y+:

$Y+=\frac{u*y}{P}$ (2)

Where P is local viscosity of fluid, nearest wall is y, and u is the friction velocity (CFD Wiki). Low Reynolds numbers correspond to low Y+ levels. It was ensured that the Y+ values on the heated walls were less than one. The Y+ values ranged from about 0.02 to 0.08. the side wall and bottom ribbed is shown in Fig. 3.7and 3.8.

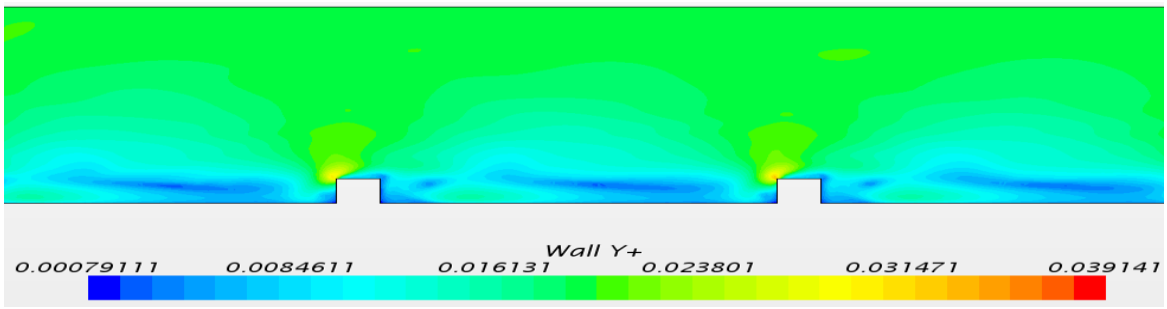

Fig.3.7 Y+ contour forthe sidewall

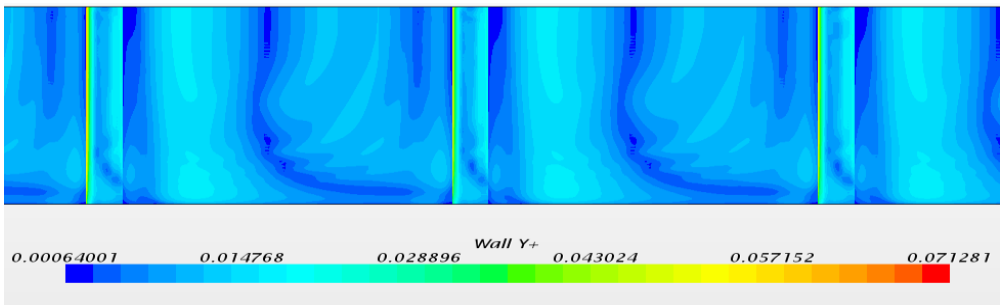

Fig.3.8 Y+contourfort he bottom ribbed wall

The realisable k- model, Menter's k- SST, the v2-f model, and the EB k- model are the turbulence models being examined in this work. The discussion of these turbulence models is skimmed over below.

Realistic k-value (rke)

The most adaptable and popular two equation industrial turbulence model in internal channels is the R k-model. The realisable k- model is an improved version of the k-model, however it is still not very suitable for flows close to the end wall. The realisable k-model is not only an advancement over the conventional k-model, but it is also a very flexible and popular turbulence model. According to the STAR-CCM+ Manual, the realisable k- model uses two equations to solve the Navier-Stokes equation for kinetic energy (k) and dissipation () values through the turbulent zone. This is because, close to the viscous sublayer, the viscous forces outweigh the turbulent forces, negating the effects of turbulence. The realisable k- model is superior since it accounts for compressibility and buoyancy as well as corrects for aberrant strain peaks that standard k- is unable to resolve (Davis, 2012). In many applications, the realisable k-model can be used as a starting point to obtain preliminary findings.

Menter's k-SST

The k model is comparable to the k-model, with the exception that it models the particular dissipation rate (k). By including a cross diffusion component close to the wall in place of the k- in the free stream, Menter recommended blending the wall distance functions. This resulted in an efficient blending of the k- and k-models. Menter's shear stress transport (SST) model, which highlightsthe sensitivity to free stream conditions, hence outperforms the traditional Wilcox model. This model is widely used in the aerospace fieldwhere the viscous flows are typically resolved and the turbulence models are appliedthroughouttheboundarylayer(STAR-CCM+Manual).

V2f

Thev²f model is also avariantofthek-εmodelwhichincludestwoadditional equations, namely the normal stress function and the elliptical function whichmore accurately predicts the effects of turbulence at the wall (Davis, 2012). It forecasts the non-local pressure-strain effects in addition to the near wall turbulence effects, which is particularly important for the precise prediction of heat transfer, skin friction, and flow separation.

EB k- (Elliptic Blending)

Manceau and Hanjalic suggested an additional variation of the k-model. The BL V2-K model is frequently for complex geometries are most reliable model.This is one of the most reliable models. Comparing the EB k-model to the regular k-model, the EB k-model predicts the near wall effects more accurately. In comparison to the SST k-turbulence model, it is also more stable.

Experimental Setup

The experimental test testing facility was constructed beginning with a straightforward smooth channel after the computational model for the rig was established on STAR-CCM+. The heat transfer temperature measurements for single inside the airfoil were replicated in test apparatus.Before the rig could be fully operational, there were a number of challenges and issues that needed to be resolved, but resolving those issues allowed the crew to get a deeper understanding of how various components function.

General RigDescription

All experiments were conducted with a consistent heat flux on the target wall at steady state conditions. As described previously two designed of test rig accomodate. The 1.5 m-long test rig was constructed from 3/4" acrylic plates with a 12 cm width. The geometry of the test section is depicted in Fig. 3.9 below.

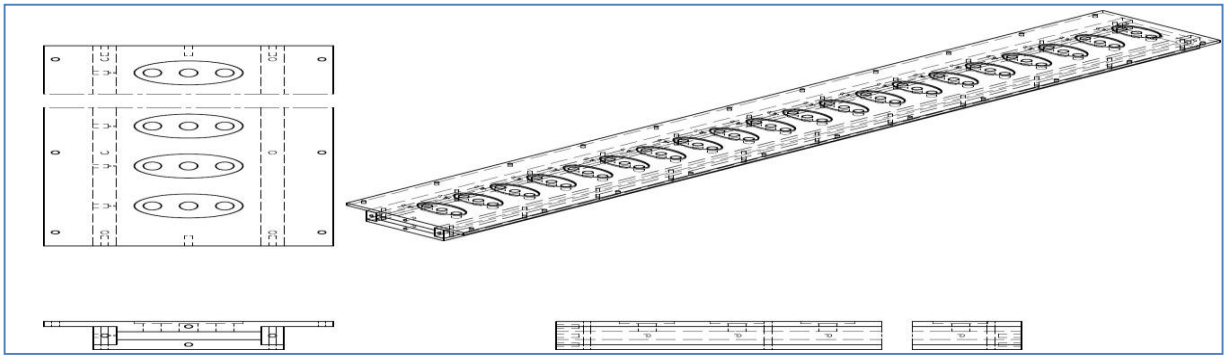

Fig.3.9 section of experimental test rig of CAD

On one end, the rig was connected to a centrifugal blower using PVC pipes, and the other end was left open to allow air to enter the test portion. The ambient air was sucked into the blower through the open end of the channel by using the blower's suction side. The amount of flow that is drawn into the blower is controlled by flow control valves. To balance the flow and prevent the blower from having to work too hard, auxiliary valves are used. The experimental blower and its piping design are shown in Fig. 3.10 below.

Fig.3.10 blower with control valves (experimentally)

Threaded studs were used to attach the side walls to the top and bottom plates, and Teflon gaskets were used to seal all joints to prevent leaks.

Static pressure taps were installed in one of the side walls to collect pressure profiles along the test rig's length. The target wall which is the bottom wall waspainted using Temperature Sensitive paint (TSP) and was then instrumented with Inconel(Grade 625) heaters constructed from a series of single heater strips each 15mm in width.

The TSP was aroused during the heat transfer experiment using two different types of LEDs—a high powered LED spot light and a succession of custom-made LED light bulbs. A reflector sheet was utilised to diffuse the LED lights equally so there wouldn't be any bright spots. According to tests, it takes roughly 15 minutes for the light intensity to stabilize. When single scientific grade CCD, thermos electrically cooled camera with zoomed lens was used. The camera was mounted on a three-axis traverse, which assisted to position it so that the photographs were taken at the proper distance. This traverse's movement in the positive and negative, X, Y, and Z directions was programmed in Matlab. A dark chamber was built using 80-20 bars and cloth to be prevent the TSP from getting damaged by exposure to common lighting.

The Uni-Coat TSP from ISSI Inc. was employed in this lab's testing. The TSP is made up of a binder, fluorescent molecules, and luminescent paint. When these molecules are appropriately stimulated, a reaction occurs that is temperature-sensitive. Using a particular camera, this shift is documented. The photos are then processed to include the whole temperature distributions applied throughout the entire length of the TSP paint. Compared to placing many thermocouples on the surface being tested, the TSP is a very accurate way to measure temperature changes. Before use TSP to be calibrated and accomplished small acrylic was adhered copper block can kept consistent temperature. The voltage applied to this block was in charge of regulating its

temperature.
Before and after the block was heated, photos were taken. From cold to hot image the heat transfer calculated. The Matlab code required to process the camera-captured intensity images is created using these calibration values.
In the same smooth channel, ribs were added to the top and bottom surfaces of the experimental test rig for the ribbed configuration. The rib height-to-hydraulic diameter (e/D) ratio was raised from 0.063 to 0.076 while maintaining the same pitch-to-rib height (P/e) of 10 as in the CFD analysis. This e/D produced square ribs with a 5 mm cross section. The ribs were cut from long aluminium 6061 bars to the necessary length. The ribs were spaced 45mm apart according to the chosen pitch, totaling 32 ribs along a 1.55m test rig. Kapton tape was used to secure these ribs to the heater strips. To make sure the ribs were cemented into position and affixed to the side walls, additional adhesive was applied to their ends.

RESULTSANDANALYSIS

Smooth Channel Validation (Experimental) (Ref)

Both the boundary layer probe and the pitot static tube were used to calculate the velocity profiles for the smooth channel. To validate the rig, these data were then contrasted with those from a CFD simulation. These velocity measurements were made in the area that was completely developed. Fig. 4.1 illustrates flow conditions in boundary layer adjacent to wall, which was the major objective of this validation.

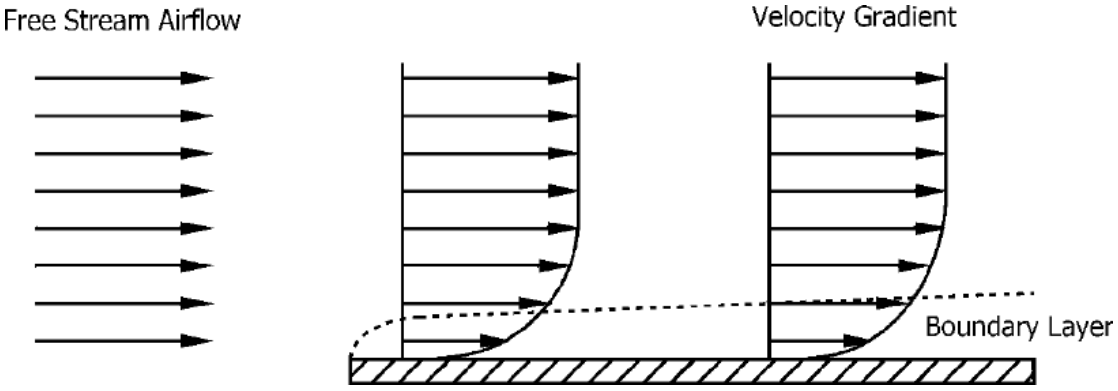

Fig.4.1 Velocity profiles at the boundary layer(Chklovski)

Expecting similar profiles, the velocity profiles for a Reynolds number of 75,000 isplotted in Fig. 4.2. Along the centerline of the test segment, the pressure readings were taken spanwise. As can be seen, because the CFD and the pitot static tube have a symmetrical profile, the velocity profile was only taken for half of the channel span and then replicated. Since the boundary layer probe is more adept at accurately foreseeing the near wall effects than the Pitot tube, it is found the boundary layer is closely match with analytical results. Additionally, by specifying a small mesh at the nearby wall and precisely resolving the boundary layer, this contributes to the validation of the computational results.

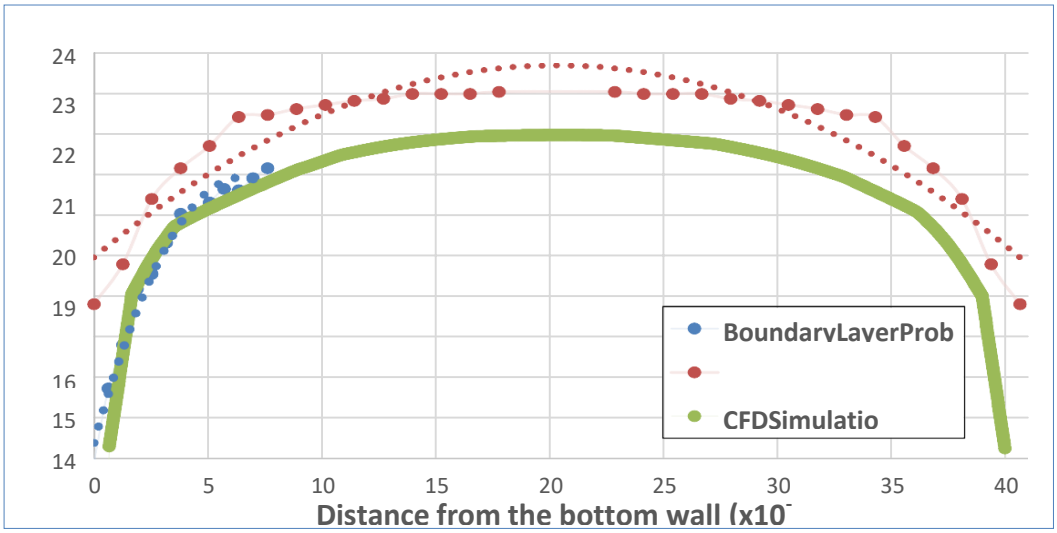

Fig.4.2 Velocity profiles of CFD vs experimental

CFD ribbed Channel benchmarking

To thoroughly examine the flow physics of the complicated flows inside the channels, CFD analysis is used. Even though CFD frequently does not produce the most accurate findings, it is used to verify the validity of experiments conducted. As previously said, setting up a smooth channel example in STAR-CCM+ to computationally investigate the fundamental findings is the first step towards the thesis's objective.

BenchmarkingtoJCHan

The goal of this section is to benchmark the experimental data from JC Han et al.(1985)workwithvariouscomputationalmodelsinSTAR-CCM+byreplicatingtheexperimental conditions. Thus, the most accurate turbulence models that nearly matched the numbers that had been published were discovered. By designating the a symmetric plane results in CFD model on top and one side wall, same as the CFD model was built up as a 1/4th structure. The computation time and resources were cut in half as a result. All of these simulations took an average of 24 hours and 15,000 iterations to complete on the ERAU Rigel network. The residuals for the EB k-turbulence model's iterations are displayed in Fig. 4.3 below, averaged across time.

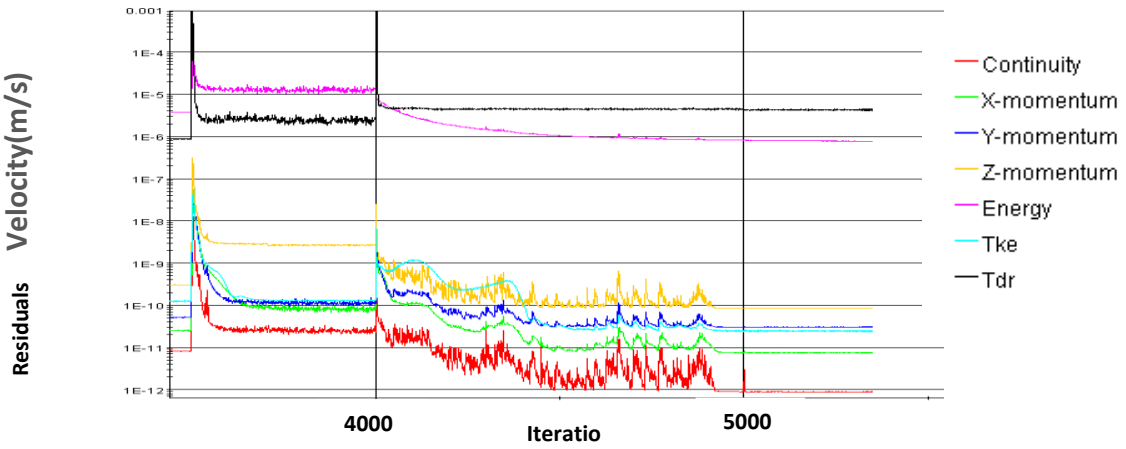

Fig.4.3 Residuals for time averaged iterations

Pressure Dataand Friction Factor

It is crucial to examine the fluid flow parameters before moving on to comprehend the heat transfer analysis of the rib effect on cooling the turbine blade. The friction factor was used to compare pressure between experimental and computer results. A dimensionless number called the Fanning friction factor is used to describe frictional losses in the channel. Different turbulence models and the Reynolds number at which the channel experiences the flow affect these losses differently.

AsseeninFig.4.4,thefrictionfactorforHan's(1985)dataatα=90°iscomparedwith smooth channel results as well as the present study for the four different turbulencemodels.

The friction factor rises with an increase in Reynolds number, as seen in the figure, because of increasing turbulence that causes higher pressure decreases. Table 4.1 computational model and experimental by JC Han are contrasted.

Table 4.1 Friction factor comparison to Han's(1985)dataPercent Diff

	Re=21,500	Re=42,000
V^2F	**5.3%**	-
Rk-ε	13.8 %	12.1%
EBk-ε	6.8 %	**5.8 %**
k-ω	9.8 %	9.4 %

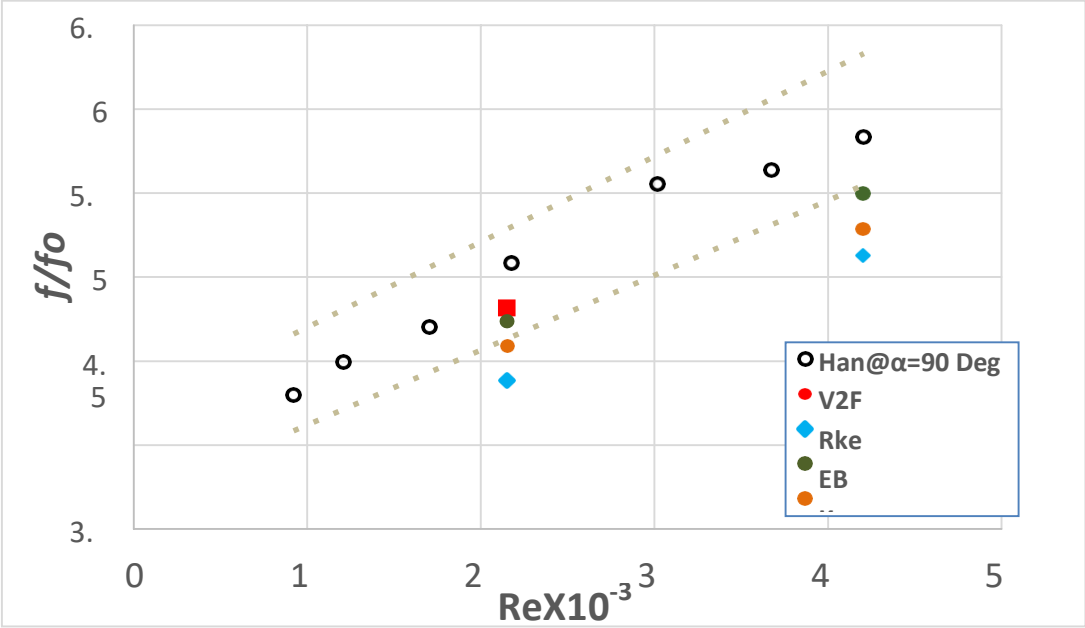

Fig. 4.4 Reynolds Number vs f/f_0

According to JC Han's data, the V2f model predicts Re @ 21,500 to be the closest to the experimental value, and Re At 42,000 to be the closest to EB k- matches, both of which are within the experimental value's 6.8% uncertainty range.

Heat Transfer Analysis

To analyze the different turbulence and compare them, Nusselt number variationswere compared along with results from Han's (1985) work. Contor plots the Nusselt number completely mesh independent models for section EB k and V_2F at steady state are

shown in Figs. 4.5 and 4.6. The EB k- displays a superior near wall prediction than the V2F model, as can be observed. Thus, as was previously observed, it exhibits more heat transmission than V2F. Additionally, V2f exhibits a notable reduction in Nu. The trend was comparable even if the Nusselt numbers differed from model to model.

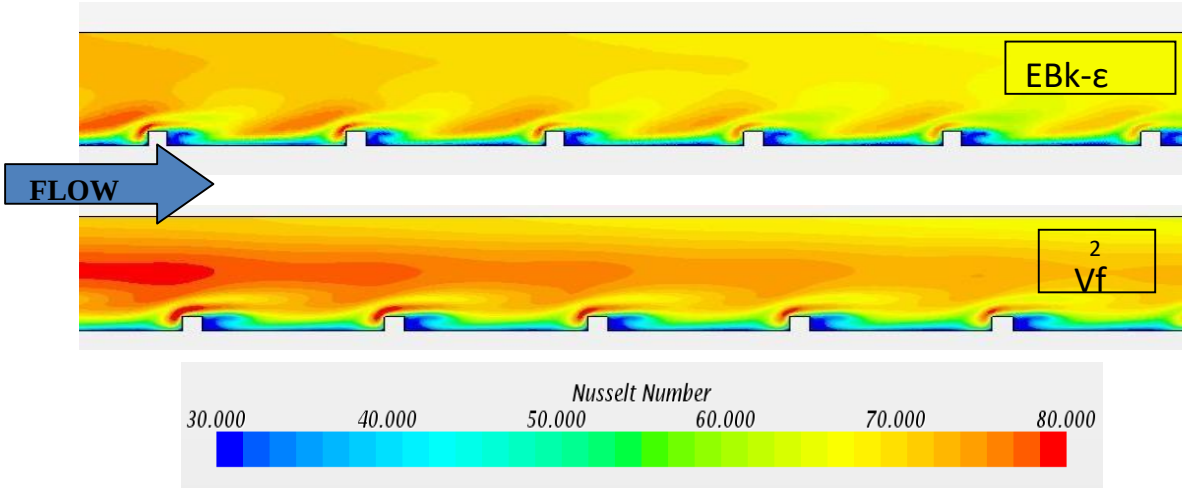

Fig.4.5 Nusselt Number contours forEBKeandV²Fmodels on thesidewall

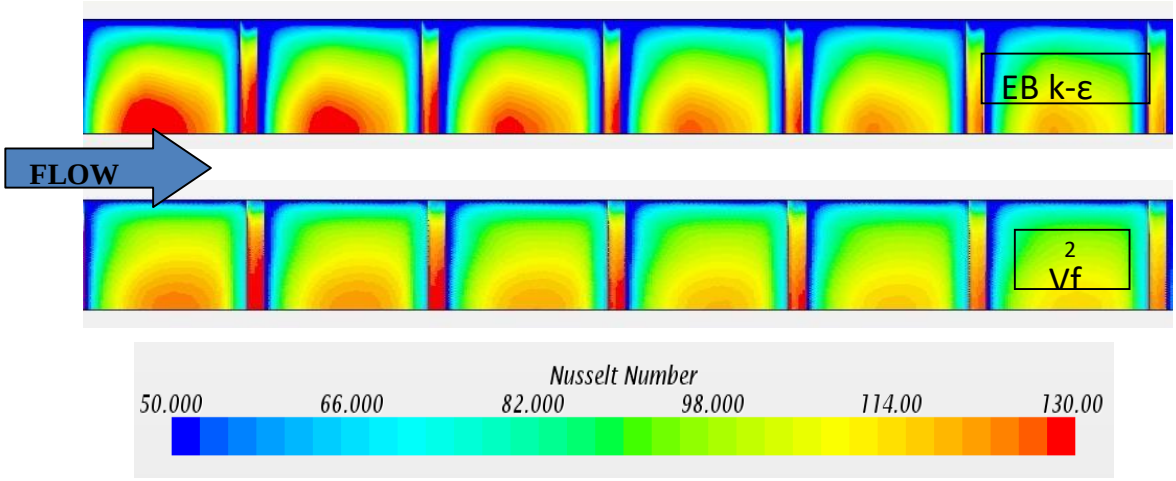

Fig.4.6 Contours for EB k vs V²F models

The contours display a high Nusselt number on the top of the rib, followed by a reduction in Nu immediately after the rib, as would be expected. The flow splits off from the main turbulent flow at this point. The flow reversal has resulted in a very low Nu in the area behind the rib. High Nu values are also seen in the area between the two ribs because there is the greatest heat transfer there since the main fluid flow comes into touch with the hot gases outside.

To collect data and analyse it, various turbulence models were used to the scenario with the greatest degree of mesh independence. After then, a Nu variation plot was created by plotting them along the length. A program in MATLAB was developed to built mean values of length and other turbulence models. The heated portion of the rig's bottom wall and rib plane are shown in Fig. 4.7 as plots of the Nu vs. length scale (X/D). The non-dimensional value of the hydraulic diameter divided by the distance in the X direction is known as X/D.

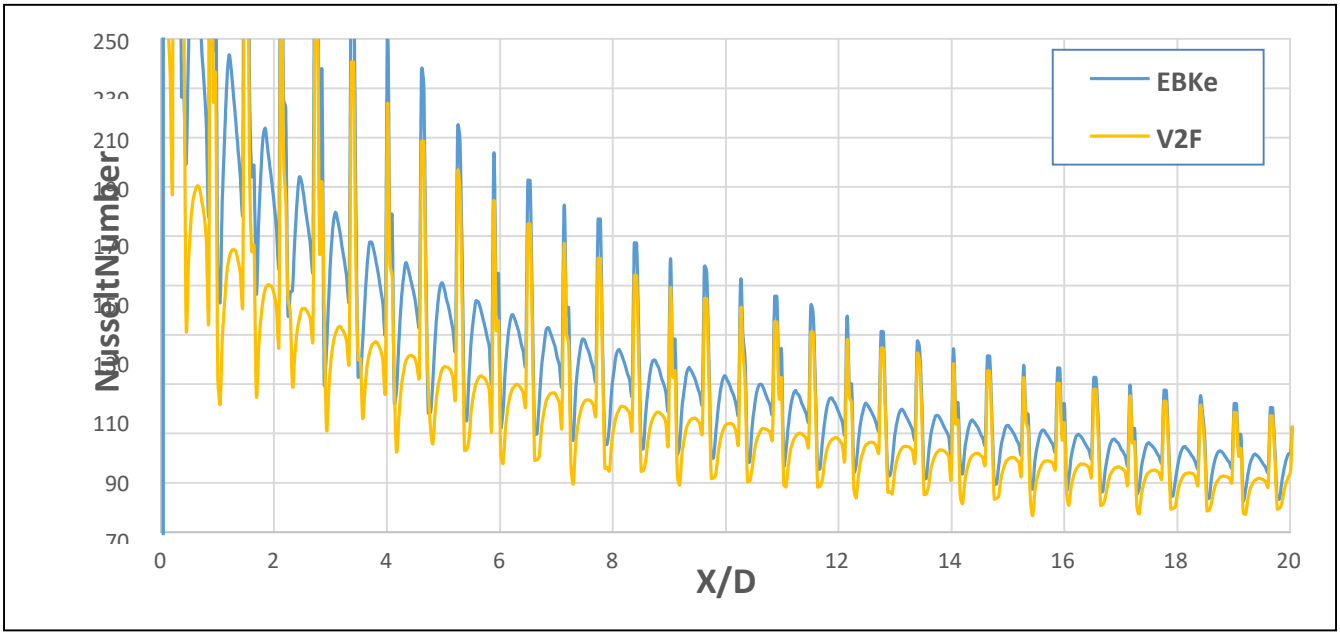

Fig.4.7 meanNusselt number span variation on ribs

The EB k-turbulence model has relatively high Nusselt numbers in the first few rows of ribs when it comes to variation on the ribs plane, but as it moves downstream, it becomes linear and occasionally completely formed. Although the Nusselt number values for the V2F turbulence models are lower, they exhibit a similar pattern to that of the EB k-. The Nusselt number on the surface of the ribs is depicted in the illustration by the spikes, while the Nu is represented by the plateau region between the ribs.

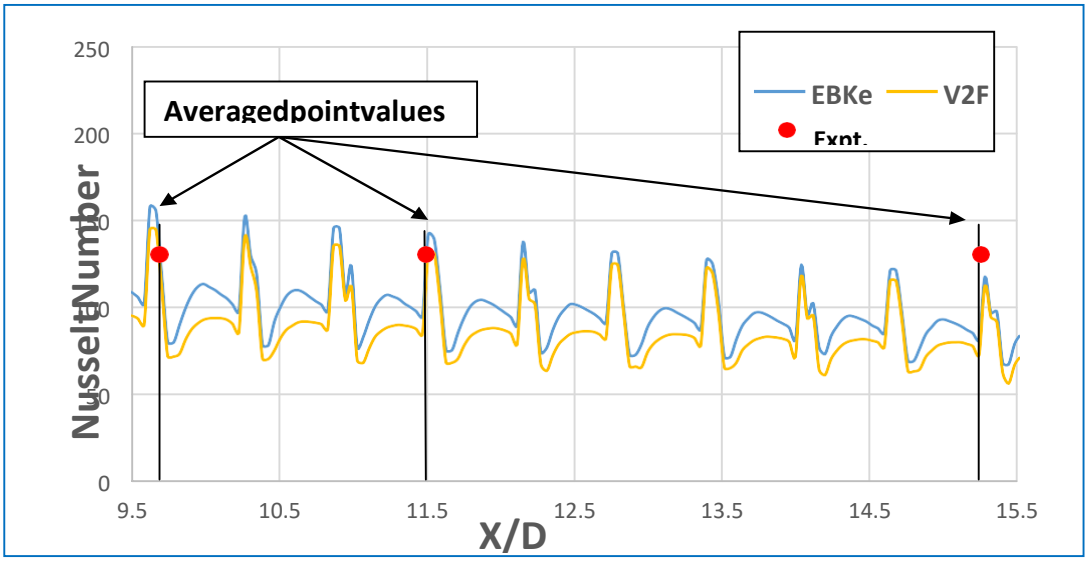

Fig.4.8 Variation for Nusselt number in fully developed region

A zoomed-in portion of the completely developed region is shown in Fig. 4.8. It shows the Nusselt numbers between X/D of 9.7 and 15.3 that have been averaged span-wise. Han's (1985) work was compared to the average of the three locations in the fully developed region. The k- and EB k- were the closest matches, with overprediction rates of 2.5% and 1.6%, respectively. The R k- and V2F models, on the other hand,

underpredicted by 7.0% and 4.7%, respectively. These values are within 6.8 percent of Han's (1985) uncertainty. Since they correctly take into account near wall effects, it can be demonstrated that all three k-model variations perform better than the realisable k-model.
Using point probes between an X/D of 9.7 and 15.3, local Nusselt numbers in the fully developed area were discovered. This was equivalent to the channel's entire length, or 0.74 to 1.16 metres. It can be noticed that the smooth side's Nusselt number is lower than those obtained at the ribbed surface. Fig. 4.9 belowgives the distribution of theNusseltnumberscomparedto Han's (1985)data in the fullydeveloped region.

Table-4.2 Local Nusselt number comparision between experimental &CFDmodels

	X/D	**9.7**	**%Error**	**11.5**	**%Error**	**15.3**	**%Error**
Rk-ε	Rib	119.5	8.4	110.2	15.5	105.7	18.9
	Smooth	63.3	13.5	58.9	19.5	57.3	21.7
EBk-ε	Rib	128.1	1.8	121.9	6.5	115.6	11.3
	Smooth	71.9	1.8	71.2	2.7	65.6	10.4
V2F	**Rib**	128.1	1.8	122.9	5.8	119.5	8.4
	Smooth	78.7	-7.5	74.9	-2.3	72.8	0.5
K-ω SST	Rib	124.2	4.8	119.5	8.4	110.2	15.5
	Smooth	68.0	7.1	63.3	13.5	62.9	14.1

Ribbed Channel Data (PTML)
CFDAnalysis
Two turbulence models, V2f and EBk-, were found after examining the computational benchmarking results to closely match the experimental values within the uncertainty. Since both models are subject to uncertainty, it is extremely challenging to determine which performs better than the other. However, based on the data, the V2f demonstrated improved matching in reattachment length and the lowest Reynolds number match but struggled higher numerical values. In order to establish the CFD model for internal validation for the experimental facility, the EBk-model was employed for the early study. The experimental test rig was duplicated in STAR-CCM+ and simulated with the same boundary conditions at Re of 21,500 and 42,000.
Fig. 4.11 illustrates Nusselt number values on bottom wall for Reynolds number 2500 to 42000 for test section. In both instances, it is observed that the Nusselt number variation diminishes as the channel lengthens. Less variance is observed between the ribs in the lower Re. This is seen because there is less turbulence created. The Nusselt number, on the other hand, peaks near the leading edge of the rib in the case of lower Re and shows a poor heat transfer rate behind the rib. The theoretical smooth channel values computed by Dittus-Boelter and Gnielinski were contrasted with the results from both of these examples. The ribbed channel gives 3 times higher Nusselt number as observed..

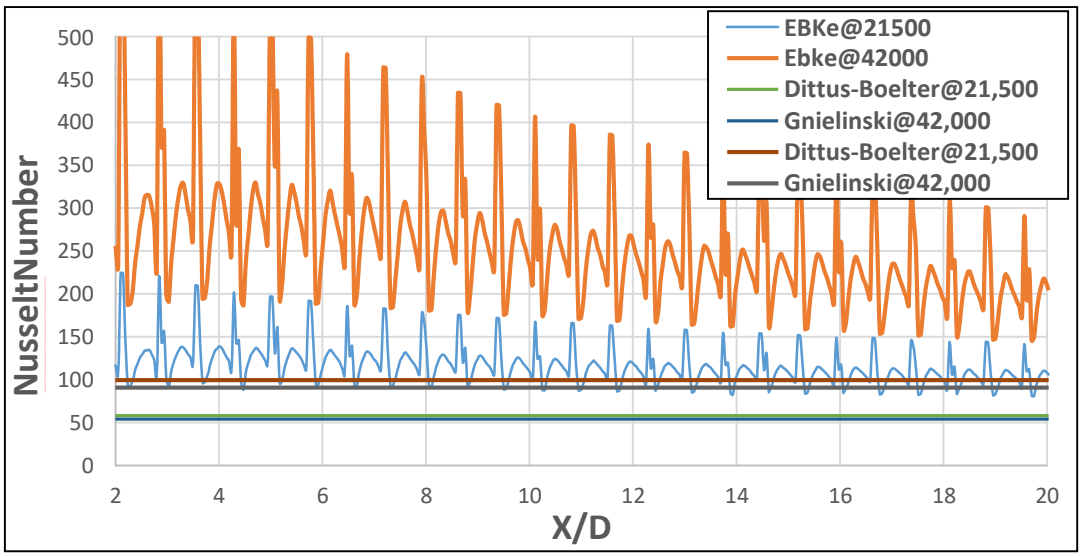

Fig.4.11 Mean Nusselt number at bottom wall computationally

The Nusselt number contours for the ribbed arrangement for the EBk-model run at a Re of 21,500 are shown in Fig. 4.12 below. It should be noticed that lateral conduction wasn't considered in the CFD calculations, hence the contours show a lower Nu at the side walls.

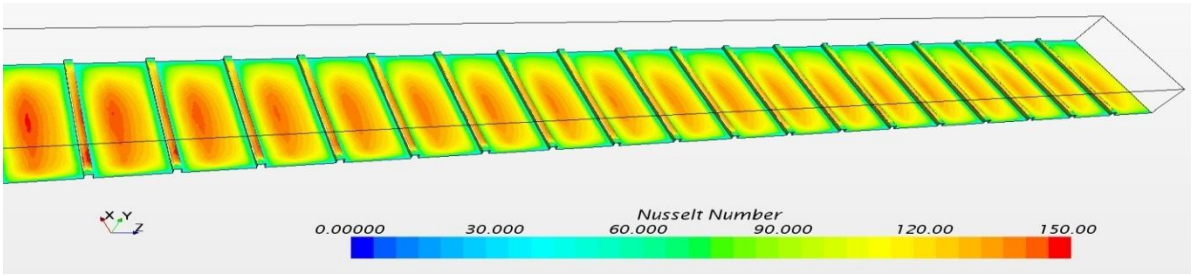

Fig.4.12 Contour Nusselt number for Re 21500

Experimental Analysis

Six separate examples were run through the test rig's experimental analysis. Three distinct heat fluxes of 566, 1670, and 2055 W/m2 were used to examine two Reynolds numbers of 21,500 and 42,000. To be consistent with the other situations tested earlier, these Reynolds numbers were chosen. At the same Nusselt number compare heat transfer rates, the heat fluxes on the opposite side were examined.

The experimental temperature contour for the test rig's streamwise direction is depicted in Fig. 4.13 below. First half of contour temperature is lower to second half at downstream channel.

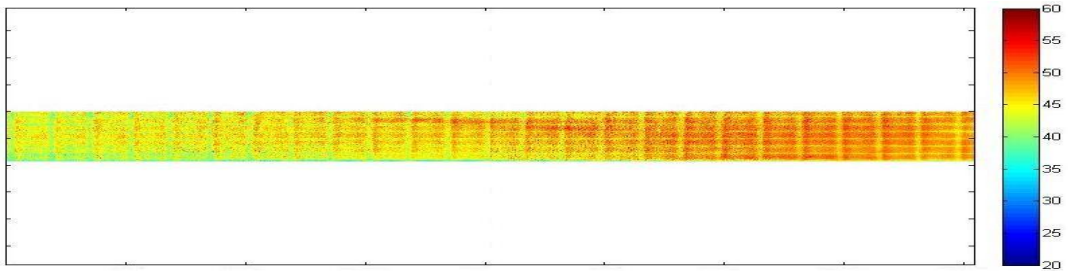

Fig.4.13 Experimental Contour forTemperature

The trends just demonstrate the reverse, much like in the case of heat transport. Down the channel, the Nusselt number starts to fall. This occurs because the air is turbulently mixed upstream of the channel, where it tends to lose its cooling ability. The Nusselt number contours for the ribbed channel at Re=21,500 and a heat flux of 1670 W/m2 are displayed in Fig. 4.14 below.

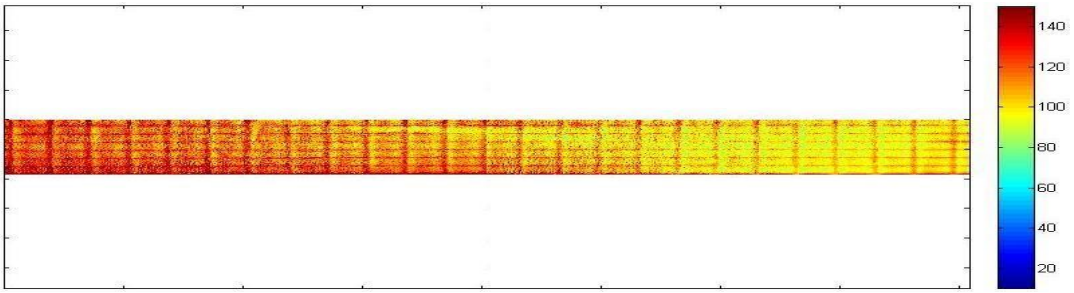

Fig. 4.14 Nusselt number experimental contour

The span averaged charts below provide a clearer view of the heat transfer rates. The values of the Nusselt numbers displayed at a Re of 21,500 and 42,000 are compared in Figures 4.15 and 4.16. The in-house PTML rig is validated at low Re since the CFD heat transfer rates closely match experimental data. Another observation is that experimental testing does not exhibit the abrupt increases in Nusselt numbers that are shown in CFD.

The Nusselt numbers charts do not line up closely in the higher Re example, indicating that there is less air mixing at higher turbulence than there is in the lower Re case. Since the value increases dramatically, the reattachment length lengthens as well, resulting in less interaction with the inner walls.

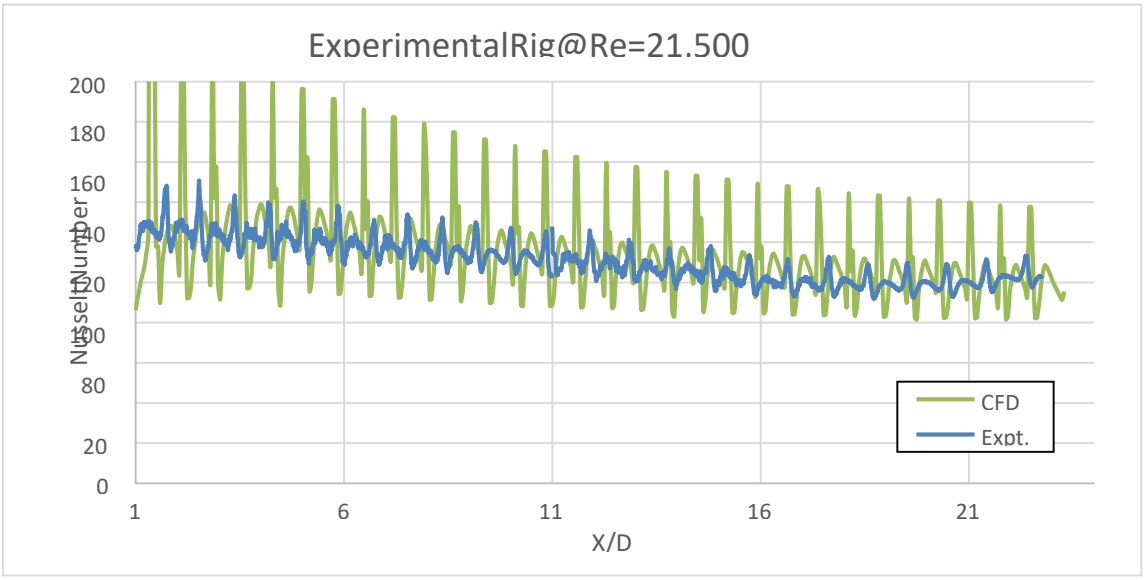

Fig. 4.15 Experimental span averaged Nusselt Number along the bottom wall atRe= 21,500

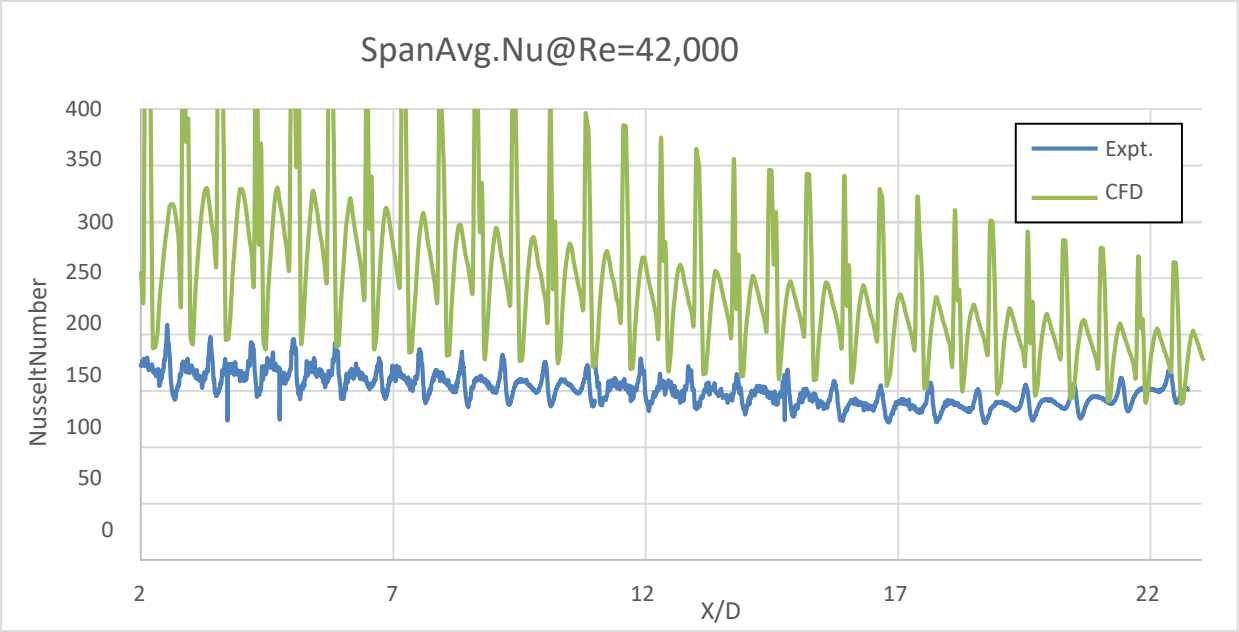

Fig. 4.16 Experimental span averaged Nusselt Number along the bottom wall at Re = 42,000

It is clear from the experimental findings below that CFD is predicted. One of the causes could be because a highly conductive aluminium rib was attached using low conductivity thermal tape. In cases of CFD, there are also unexpected spikes at the leading edge of the rib because lateral conduction was not taken into account.

CONCLUSIONAND RECOMMENDATION

Conclusion

This research's objective was to compare the experimental findings of J. C. Han to those of computational fluid dynamics (CFD) in a channel with rub turbulators while also analysing the flow conditions. Following the previous benchmarking, the optimum flow conditions are employed to validate an internal experimental rig for additional optimization investigations. Comparing four widely used turbulence models revealed that the V2F turbulence model produced the best results for a periodic ribbed channel with P/e = 10 and e/D = 0.063.This turbulence model underpredicted the friction factor by roughly 5.3 percent and matched experimental results from Han's (1985) data within 5% of the experimental local Nusselt numbers. Even though EB k- was not particularly near to the literature value in the instance of the variation in reattachment lengths, it nevertheless demonstrated increased heat transfer rates between the ribs. These examples will run independent mesh where Y+ case consist smaller to one.

Friction factor comparison was done to validate the pressure profiles. In case ofthe EB k-ε turbulence model, both higher and lower Reynolds number values were withinthe uncertainty of Han's (1985) work. Before the best match can be found, more research is required to examine multiple turbulence models with various Reynolds values and rib placements in the channel.

V2F and EB k- were the two turbulence models that matched the data the best. Higher Reynolds values were reached before V2F began to deviate because of its extreme instability. Consequently, the EB k-turbulence model was applied to all of the remaining examples. The experimental outcomes at a Re of 21,500 very closely matched the CFD outcomes, validating the PTML rig testing facility. The goal of computationally

validating the rig aids in minimising considerable experimentation with various setups. Different boundary conditions can be simulate using CFD.
The cooling technology and turbine engine are the subject of extensive study. The turbine inlet temperature can be raised to increase efficiency. This effort was done to improve the interior channels of a turbine blade employing rib tabulators with that objective in mind. The results of this study's data analysis make it clear that rib turbulated cooling improves heat transfer while minimising pressure loss, leading to higher operational turbine intake temperatures.

Recommendations
After the experimental rig has been validated with CFD, it will be fascinating to look into additional research on rib turbulated cooling. After considering various shapes and combinations, rib optimization would be the next development in rib roughed cooling. Using the STAR-CCM+ plugin OPTIMATE+, a preliminary optimization study was conducted in collaboration with the Undergraduate research team (IGNITE). As a result, the user may improve the rib across several disciplines. To look at faster heat transfer rates, various shapes and rib arrangements can be examined. Therefore, future research towards rib optimization should be considered.

Symbols

ε	Strain Energy or Turbulent Dissipation Rate (Tdr)
η	Efficiency
□	Per unit strain energy
D	Hydraulic dia
f	Friction Factor
H	Coefficient of heat transfer
I	Paint intensity
Ir	Paint intensity of reference image
kair	Air thermal conductivity
kI	Inconel thermal conductivity
K	Kinetic energy of turbulent (Tke)
M	Mach number
M	Fluid flow rate
Nu	Nusselt number
Pr	Prandtl number
Ps	Static pressure
P0	Total pressure
Re	Reynolds number
Sc	SchmidtNumber

T	Temperature
T3	Temperature turbine inlet
T4	Temperature turbine exit
Tw	Wall temperature
Tr	Fluid reference temperature
x	Distance in Streamwise direction
X/D	Streamwise distance in terms of hydraulic diameter

REFERENCES

1. Bredberg, Jonas. "Turbulence Modelling for Internal Cooling of Gas-Turbine Blades."Web.15 Sept. 2015.
2. Buchlin,Jean-Marie."ConvectiveHeatTransferinaChannelwithPerforatedRibs."
3. *International Journal of ThermalSciences*41.4(2002):332-40.Web.
4. Chandra P. R.; Alexander C. R.; Han J. C.; 2003 "HeatTransfer and Friction Behaviorsin Rectangular Channels with Varying Number of Ribbed Walls", International Journal of Heat and Mass Transfer, Vol.46, pp. 481-495.
5. Chklovski,Tara."Pointed-TipWingsatLowReynoldsNumbers."*Www.wfis.uni*.N.p., n.d. Web.
6. Clifford,R.J.,1985."RotatingHeatTransferInvestigationsonaMultipassCoolingGeometry."AGARDCP 390.
7. Davis, P. L., A. T. Rinehimer, and M. Uddin. *"A Comparison of RANS-Based TurbulenceModelingforFlowoveraWall-MountedSquareCylinder|CD-adapco."*AComparisonofRANSBasedTurbulenceModelingforFlowoveraWallMountedSquareCylinder |CD-adapco*.CD-Adapco, 2012.Web. 08June2015.*
8. Dhanasekaran, T.s., and Ting Wang. "Computational Analysis of Mist/air Cooling in aTwo-pass Rectangular Rotating Channel with 45-deg Angled Rib Turbulators."*InternationalJournal of Heatand Mass Transfer*(2013): 554-64. Print.
9. Dimensionless Wall Distance (y Plus). -- *CFD-Wiki, the Free CFD Reference*. Web. 2Oct.2015.
10. Ekkad, S. V. and Han, J.-C., "Detailed Heat Transfer Distributions in Two-Pass SquareChannels with Rib Turbulators," International Journal of Heat and Mass Transfer,Vol. 40, No. 11, 1997, pp. 2525–2537
11. Florschuetz, L. W., Truman, C. R., Metzger, D. E., "Streamwise Flow and Heat TransferDistributionsforJetArrayImpingementwithCrossflow,"JournalofHeatTransfer,Vol. 103, 1981,pp. 337.
12. Flynt,GuyA.,RobertS.Webster,andKidambiSreenivas."ComputationofHeatTransfer in Turbine Rotor Blade Cooling Channels with Angled Rib Turbulators."*49thAIAA/ASME/SAE/ASEE JointPropulsionConference*(2013).Print.
13. Han J. C.; Glicksman L. R.; Rohsenhow W. M.; 1978 "An Investigation of Heat Transferand Friction for Rib-Roughened Surfaces", International Journal of Heat MassTransfer,Vol. 21, pp. 1143-1156.
14. Han,J.C.,J.S.Park,andC.K.Lei."Heat Transfer Enhancement in Channels with TurbulencePromoters."*JournalofEngineeringforGasTurbinesandPower*107(1985): 628.Print
15. Han, J.C., 1988, "HeatTransfer and Friction Characteristics in Rectangular ChannelswithRibTurbulators,"ASMEJournalofHeat Transfer,110, pp.321-328.

16. Han, J.C. and Park, J.S., 1988, “Developing Heat Transfer in Rectangular Channels withRibTurbulators” InternationalJournalofHeatand MassTransfer,31pp.183-195.
17. HanJ.C.,S.Dutta,andS.V.Ekkad,“GasTurbineHeatTransferandCoolingTechnology,”Tay lor &Francis,Inc.,New York(2000)
18. Han, J.C., and Chen, H.C., 2006, “Turbine Blade Internal Cooling Passages with RibTurbulators,”J.ofPropulsionandPower,Vol. 22,No.2,pp.226-248.
19. Han, J.C., Zhang, Y.M., and Lee, C.P., 1991, “Augmented Heat Transfer in SquareChannels with Parallel, Crossed, and V-Shaped Angled Ribs,” ASME Journal ofHeatTransfer, 113, pp. 590-596.
20. HyungHee Cho, Kyung Min Kim, JiwoonSong,“ApplicationsofImpingementJetCooling Systems.” Department of Mechanical Engineering, YonseiUniversity,Seoul,Korea, 2011.
21. Kim,Hong-Min,andKwang-YongKim."ShapeOptimizationofThree-dimensionalChannel Roughened by Angled Ribs withRANS Analysis of Turbulent HeatTransfer."*International Journal ofHeat and MassTransfer*: 4013-022. Print.
22. Kim, Kwang-Yong, and Sun-Soo Kim. "Shape Optimization of Rib-roughened Surface toEnhanceTurbulentHeatTransfer."*InternationalJournalofHeatandMassTransfer*:27 19-727. Print.
23. Kim,KyungMin,YunYoungKim,DongHoRhee,andHyungHeeCho.*"AnInvestigation of Duct Aspect Ratio Effects on Heat/Mass Transfer in a RotatingDuctwith 90°Ribs."*ASME TurboExpo 2004 *3(2004):483-92.Web.*
24. Kiml, Robert, Sadanari Mochizuki, and Akira Murata. "Effects of Rib Arrangements onHeatTransferandFlowBehaviorinaRectangularRib-RoughenedPassage:Application to Cooling of Gas Turbine Blade Trailing Edge." *Journal of HeatTransfer*123.4 (2001): 675-81. Web.
25. Iacovides, H., and B.e. Launder. "Computational Fluid Dynamics Applied to InternalGas-turbine Blade Cooling: A Review." *International Journal of Heat and FluidFlow*:454-70. Print.
26. Park,J.S.,Han,J.C.,Huang,Y.,Ou,S.,andBoyle,R.J.,1992,“HeatTransferPerformanceComp arisonsofFiveDifferentRectangularChannelswithParallelAngledRibs,”InternationalJ ournalofHeatandMassTransfer,35,pp.2891-2903.
27. Rau, g.;Çakan, M.;Moeller, D.; Arts,T.; 1998 “The EffectOf Periodic Ribson theLocalAerodynamicandHeatTransferPerformanceofaStraightCoolingChannel”,AS MEJournal of Turbomachinery, 120, pp368-375.
28. Ricklick, Mark A., andCassandra Carpenter. "Comparison of Heat Transfer PredictionforVariousTurbulenceModelsinaPinFinChannel."*50thAIAA/ASME/SAE/AS EE Joint Propulsion Conference*(2014).Print.
29. Ricklick, Mark. "Characterization of an Inline Row Impingement Channel for TurbineBladeCoolingApplications."Web. 18 July2015.
30. RobertoClaretti,MarkRicklickandJ.S.Kapat,“ComputationalandExperimentalCompar isonofHeatTransferCharacteristicsofaTripleRowImpingementChannelatLargeImpin gementHeights”.CenterforAdvancedTurbinesandEnergyResearch, 2011
31. STAR-CCM+ Version 9.02.007 User Guide, CD-adapco Inc., New York, 2013.Sundberg,Jenny."HeatTransferCorrelationsforGasTurbineCooling."Web.11July 2015.
32. Taslim, M. E., K. Bakhtari, and H. Liu. "Experimental and Numerical Investigation ofImpingementona Rib-RoughenedLeading-Edge Wall." *J. Turbomach.JournalofTurbomachinery*: 682. Print.
33. Taylor, J.R., “Heat Transfer Phenomena in Gas Turbines.” ASME Turbo Expo, GT-

172,ASME,New Orleans,LA, 1980
34. Wang L. B.; Tao W.; Wang Q.; Wong T. T.; 2001 “Experimental Study of DevelopingTurbulent Flow and Heat Transfer in Ribbed Convergent/Divergent Square Duct”,InternationalJournalofHeat and Flow, Vol. 22,pp.603-613.
35. *Wikipedia*.WikimediaFoundation.Web.30Sept. 2015.
36. Zhang, Q., P. M. Ligrani, and S. W. Lee. "Determination of Rough-surface Skin FrictionCoefficients from Wake Profile Measurements." *Experiments in Fluids* (2003):627-35. Print.
37. ZuckermanN.,LiorN.,“ImpingementHeatTransfer:Co-relationsandNumericalModeling”.InternationalJournalof HeatTransfer,2005
38. Dharamveer, Samsher, Singh D.B., Singh A.K., Kumar N. (2019) “Solar Distiller Unit Loaded with Nanofluid—A Short Review”. In: Kumar M., Pandey R., Kumar V. (eds) Advances in Interdisciplinary Engineering. Lecture Notes in Mechanical Engineering. Springer, Singapore. pp 241-247, Paper Published. Scopus Index, Springer Publication.https://doi.org/10.1007/978-981-13-6577-5_24
39. Dharamveer, Samsher “Comparative Analysis of Energy Matrices and Enviro-economics for Active and Passive Solar Still”. Journal Materials Today proceedings, Elsevier publication. https://doi.org/10.1016/j.matpr.2020.10.001